

s*-Wave $I=0$ $\pi\pi$ Resonance

Bryan F. Gore

*Center for Theoretical Physics, Department of Physics and Astronomy,
University of Maryland, College Park, Maryland 20742**and Central Washington State College, Ellensburg, Washington 98926*

(Received 17 August 1970; revised manuscript received 3 April 1972)

Solutions are presented for subtracted dispersion relations, written for the s - and p -wave inverse $\pi\pi$ scattering amplitudes with poles inserted into both s waves. These solutions predict the existence of a broad $I=0$ s -wave resonance (σ) accompanied by a small, negative $I=2$ phase shift, in the absence of any s -wave experimental input. While p -wave subtraction parameters are adjusted to fit a 755-MeV ρ resonance with width 120 MeV, the s -wave parameters are determined by crossing symmetry through derivative conditions to third order. The coupling constant, λ , is a free parameter, and resonant solutions are obtained for $-0.033 \leq \lambda \leq 0.040$ with σ masses ranging from 550 to 900 MeV. Both s -wave amplitudes exhibit zeros between the cuts for $-0.01 < \lambda < 0.02$, and for $\lambda = -0.008$ the zeros coincide with those predicted by the Adler condition applied on the mass shell. Solutions with $\lambda \lesssim -0.01$ satisfy crossing conditions for $\pi^0\pi^0$ amplitudes. The failure of the other solutions to satisfy them may be related to approximations made in applying crossing symmetry. A method of improving the solutions is suggested.

I. INTRODUCTION

In this paper calculations of subtracted dispersion relations written for the s - and p -wave inverse $\pi\pi$ scattering amplitudes are presented. Elastic unitarity is used in the evaluation of right-cut integrals, and approximate crossing symmetry in the evaluation of left-cut integrals. s -wave parameters are evaluated using derivative conditions from approximate crossing symmetry, and the two p -wave subtraction constants are fixed by requiring a p -wave resonance of mass 755 MeV and width 120 MeV, the ρ . The Chew-Mandelstam coupling constant, λ , is treated as a free parameter, and orders the solutions.

Pole terms are inserted into the s -wave inverse amplitudes, and allow the possibility of zeros in both s -wave partial-wave amplitudes. While such zeros have been predicted from PCAC (partially conserved axial-vector current) considerations,¹ no conditions from current algebra are imposed in these calculations. For solutions obtained, the positions of the zeros of the $I=0$ and 2 s -wave amplitudes, plotted one against the other, lie on a straight line passing through the point predicted by PCAC.

Solutions are presented for the range $-0.03 < \lambda < 0.10$. Within the range $-0.03 < \lambda < 0.04$ these solutions exhibit an $I=0$ s -wave resonance, the σ , with mass increasing from 550 MeV for $\lambda = -0.033$ to 900 MeV for $\lambda = 0.04$. The expected weakening of the interaction with increasing λ is seen in the behavior of the resonance mass, and in a transition solution (δ_0^0 small and negative below 700 MeV,

small and positive above) for $\lambda = 0.100$ linking the resonant solutions to repulsive s -wave dominant solutions previously reported for large positive λ .²⁻⁴ The $I=0$ s -wave phase shift is constrained from passing through 180° above the resonance energy since the inverse amplitude contains only one pole term.

A series of calculations leading to the results noted above is presented here. With λ fixed *a priori*, five conditions are necessary to evaluate the six s -wave parameters introduced by subtractions and pole terms. To second derivatives in the s waves, approximate crossing symmetry yields four conditions, and a single third-derivative condition has been previously derived by the author⁵ (Ref. 5 will henceforth be referred to as I). Since the third-derivative condition is difficult to apply to the inverse amplitudes, initially it was not used to evaluate parameters in the calculations reported here. Instead, first, a σ resonance of mass 745 MeV was required. In the solutions thus obtained, the s -wave $I=2$ phase shift at the mass of the ρ resonance varied (as a function of λ) over the range $-43^\circ \leq \delta_0^2 \leq -13^\circ$. The third-derivative equation was satisfied by a solution with $\delta_0^2 = -19^\circ$.

Next, the σ condition was removed and the value of δ_0^2 at the ρ mass was fixed. Solutions were obtained for δ_0^2 values of -20° , -15° , and -10° . In those solutions exhibiting an $I=0$ s -wave resonance, the mass of the σ was found to depend on both the value of λ and the value at which δ_0^2 was fixed. However, for each choice of δ_0^2 , the third-derivative condition was satisfied by only one solution. Examination of the three solutions satisfying

this condition revealed the already described correlation of resonance mass with λ . This demonstration that the imposition of the third-derivative crossing condition allowed the selection of solutions with $I=0$ s waves having a sensible dependence on λ (including one in excellent agreement with experiment), provided sufficient motivation to impose it in place of any condition from experiment. When this was done the iterations converged, yielding the resonant solutions varying appropriately with λ which have already been described.

II. FORMALISM

In terms of the variable $\nu = s/4 - 1$, where s is the center-of-mass energy squared (natural units, $m_\pi = 1$), the unitarity condition for elastic scattering is

$$A_I^f(\nu) = [(\nu+1)/\nu]^{1/2} (\cot \delta_I^f - i)^{-1}, \quad (1)$$

where $\nu > 0$ and the phase shifts, δ_I^f , are real. This relation is assumed valid within the energy range of these calculations. The once-subtracted dispersion relations for the s -wave inverse amplitudes $F_I(\nu) = A_0^f(\nu)^{-1}$, with pole terms inserted, are

$$F_{I=0,2}(\nu) = \alpha_I + \beta_I \nu / (1 - \gamma_I \nu) + f(\nu) + L_I(\nu) - i g_I(\nu) \quad (2)$$

and the twice-subtracted p -wave dispersion relation, written for $F_1(\nu) = \nu A_1^f(\nu)^{-1}$ is

$$F_1(\nu) = \alpha_1 + \beta_1 \nu + \nu f(\nu) + L_1(\nu) - i \nu g_1(\nu). \quad (3)$$

[$F_1(\nu)$ lacks the threshold pole of $A_1^f(\nu)^{-1}$.] The integral over the right-hand-cut discontinuity (given by unitarity) is

$$\begin{aligned} f(\nu) &= -\frac{\nu}{\pi} P \int_0^\infty \frac{[\nu' / (\nu' + 1)]^{1/2}}{\nu'(\nu' - \nu)} d\nu' \\ &= \frac{2}{\pi} \left(\frac{\nu}{\nu+1} \right)^{1/2} \ln [(|\nu+1|)^{1/2} + (|\nu|)^{1/2}] \\ &\quad \text{for } \nu > 0 \text{ or } \nu < -1 \\ &= \frac{2}{\pi} \left(\frac{-\nu}{1+\nu} \right)^{1/2} \tan^{-1} \left(\frac{1+\nu}{-\nu} \right)^{1/2} \text{ for } -1 < \nu < 0. \end{aligned} \quad (4)$$

The integral over the left-hand-cut discontinuity is

$$L_I(\nu) = -\frac{\nu^{I+1}}{\pi} P \int_{-\infty}^{-1} \frac{\text{Im} A_I^f(\nu') d\nu'}{\nu'(\nu' - \nu) |A_I^f(\nu')|^2}, \quad (5)$$

and the imaginary parts of the inverse amplitudes are

$$g_I(\nu) = \left(\frac{\nu}{\nu+1} \right)^{1/2} \theta(\nu) + \frac{\text{Im} A_I^f(\nu)}{|A_I^f(\nu)|^2} \theta(-\nu-1). \quad (6)$$

Using approximate crossing symmetry, the left-hand-cut discontinuity is expressed in terms of the right-hand-cut discontinuity in the crossed channels:

$$\begin{aligned} \text{Im} A_I^f(\nu) &= \frac{2}{\nu} \int_0^{\nu-1} d\nu' P_I \left(1 + 2 \frac{\nu'+1}{\nu} \right) \\ &\quad \times \sum_{I'} \chi_{II'} \sum_{l'} (2l'+1) P_{l'} \left(1 + 2 \frac{\nu+1}{\nu'} \right) \text{Im} A_{I'}^{f'}(\nu'), \end{aligned} \quad (7)$$

where χ is the usual crossing matrix

$$\chi = \begin{pmatrix} \frac{1}{3} & 1 & \frac{5}{3} \\ \frac{1}{3} & \frac{1}{2} & -\frac{5}{6} \\ \frac{1}{3} & -\frac{1}{2} & \frac{1}{6} \end{pmatrix} \quad (8)$$

and the partial-wave expansion is truncated after p waves. On the right-hand cut, $\text{Im} A_I^f(\nu)$ may be written using the unitarity condition as soon as $\text{Re}[A_I^f(\nu)^{-1}]$ is known. Hence iteration proceeds by neglecting $L_I(\nu)$ and evaluating parameters, then computing $L_I(\nu)$, recomputing parameters, etc., until all parameters change by less than 1% in the last iterative loop.

The eight parameters introduced by pole terms and subtractions are evaluated by a combination of conditions from crossing symmetry and experiment. The p -wave subtraction constants are fixed by the mass and width of the ρ resonance by requiring

$$\left(\frac{\nu^3}{\nu+1} \right)^{1/2} \cot \delta_1^1 \Big|_{\nu_\rho} = 0 \quad (9)$$

and

$$\frac{d}{d\nu} \left(\frac{\nu^3}{\nu+1} \right)^{1/2} \cot \delta_1^1 \Big|_{\nu_\rho} = -\frac{1}{\gamma} \left(\frac{\nu_\rho^3}{\nu_\rho+1} \right)^{1/2} \quad (10)$$

with $\nu_\rho = 6.25$ and $\gamma = 1.15$, corresponding to a resonance of mass 755 MeV and width 120 MeV. Thus, at the ρ resonance the p wave has the same slope as if it were given by the Breit-Wigner form

$$A_1^1(\nu) = \left(\frac{\nu+1}{\nu} \right)^{1/2} \frac{\gamma}{\nu_\rho - \nu - i\gamma}. \quad (11)$$

Crossing symmetry, applied at the symmetry point of the Mandelstam triangle, provides derivative conditions which may be used to evaluate parameters. Although an infinite number of conditions are available, higher partial waves become more important in higher-derivative conditions. (This is because the argument of the Legendre polynomials used in the partial-wave expansion contains the variable ν ; the point is more completely discussed in I.) Under the assumption that d and higher partial waves are small at the sym-

metry point, they may be neglected in the zeroth- and first-derivative equations with little effect. The resulting approximate crossing conditions, to be evaluated at the symmetry point $\nu_{sp} = -\frac{2}{3}$, are

$$2A_0^0 = 5A_1^2, \quad (12)$$

$$\frac{dA_0^0}{d\nu} = -9A_1^1, \quad (13)$$

$$\frac{dA_0^2}{d\nu} = \frac{9}{2}A_1^1. \quad (14)$$

To derive a second-derivative condition of corresponding accuracy, Chew and Mandelstam⁶ reduced the d -wave effects by approximating each d wave by a one-parameter fit at threshold. They then combined the three independent second-derivative equations to eliminate the d waves, obtaining the following approximate crossing condition for application at the symmetry point:

$$\frac{d^2A_0^0}{d\nu^2} - \frac{5}{2} \frac{d^2A_0^2}{d\nu^2} = 27A_1^1 + 18 \frac{dA_1^1}{d\nu}. \quad (15)$$

Proceeding in this spirit, in I a single approximate third-derivative equation was derived by approximating each d wave by a two-parameter threshold fit, the f wave by a one-parameter threshold fit, and removing the five parameters by combining equations. This approximate crossing condition, to be evaluated at the symmetry point, is

$$-\frac{1}{3} \left(\frac{d^3A_0^0}{d\nu^3} - \frac{5}{2} \frac{d^3A_0^2}{d\nu^3} \right) = \frac{675}{8} A_1^1 + \frac{225}{4} \frac{dA_1^1}{d\nu^2} + \frac{75}{4} \frac{d^2A_1^1}{d\nu^2}. \quad (16)$$

Further details and discussion are to be found in I. Due to the attention devoted to removing the effects of higher partial waves from higher-derivative conditions, it is assumed that the errors incurred in applying Eqs. (15) and (16) are no greater than those in Eqs. (12) through (14), so that their detailed application is indeed meaningful. An *a posteriori* discussion of errors is to be found in Sec. IV of this paper.

Before discussing the application of these conditions it is perhaps in order to comment upon their usefulness. In Ref. 7, Tryon comments that when d waves are kept, the solutions of partial-wave dispersion relations satisfy second- and all higher-derivative conditions identically; thus they are not useful to him in determining parameters. Within the formalism used here, unless the pole-term parameters are chosen to satisfy a given condition there is clearly no reason to expect it to be satisfied. Thus, for instance, the solutions here reported which were obtained without enforcing the

third-derivative condition failed, in general, to satisfy it. Since the second- and third-derivative conditions enable the determination of parameters necessary for calculation they are useful within this formalism.

Although it may not be immediately obvious, the application of the derivative equations to determine parameters is straightforward. First the conditions are expressed in terms of the inverse functions F_l . With λ specified *a priori*, the zeroth- and first-order equations provide four conditions, each linear in only one of the s -wave functions $F_{0,2}$ (recall that the p wave is completely known from the ρ mass and width):

$$\lambda = -(5F_0)^{-1} \quad (17)$$

$$= -(2F_2)^{-1}, \quad (18)$$

$$\frac{dF_0}{d\nu} = -6(25\lambda^2 F_1)^{-1}, \quad (19)$$

$$\frac{dF_2}{d\nu} = 3(4\lambda^2 F_1)^{-1}. \quad (20)$$

While differentiation of the numerically evaluated left-cut integrals is difficult after integration, Eq. (5) may be differentiated any number of times prior to the integration. Since the resulting integrals converge even more rapidly, no accuracy is lost by this procedure.

The second- and third-derivative conditions are slightly more complicated to apply because they involve both s waves. Nevertheless, when a condition from experiment is applied to either one of the s waves, that condition plus two of the conditions [Eqs. (17)–(20)] allow the evaluation of the three parameters of that partial wave via linear equations. With one s wave known, the second-derivative condition [incorporating Eqs. (17)–(20)],

$$\frac{d^2F_0}{d\nu^2} - \frac{2}{5} \frac{d^2F_2}{d\nu^2} = -(5\lambda F_1)^{-2} \left(12 \frac{dF_1}{d\nu} - \frac{81}{10\lambda} \right), \quad (21)$$

may be linearly combined with the other two equations above, specifying all parameters unambiguously. The third-derivative equation [expressed incorporating Eqs. (17)–(20)],

$$\begin{aligned} \frac{d^3F_0}{d\nu^3} - \frac{2}{5} \frac{d^3F_2}{d\nu^3} - \frac{18}{5\lambda F_1} \left(2 \frac{d^2F_0}{d\nu^2} + \frac{d^2F_2}{d\nu^2} \right) - \frac{7F_1^{-3}}{12} \left(\frac{9}{5\lambda} \right)^4 \\ = 3(\lambda F_1)^{-2} \left[\left(\frac{1}{2} \frac{d^2F_1}{d\nu^2} \right) - \frac{1}{F_1} \left(\frac{dF_1}{d\nu} \right)^2 \right], \end{aligned} \quad (22)$$

may then be evaluated straightforwardly.

When Eq. (22) is used in solving for parameters, a quadratic equation results for the ratio γ_I/β_I for one of the s waves. Consequently, two sets of parameters are produced. In general, initially

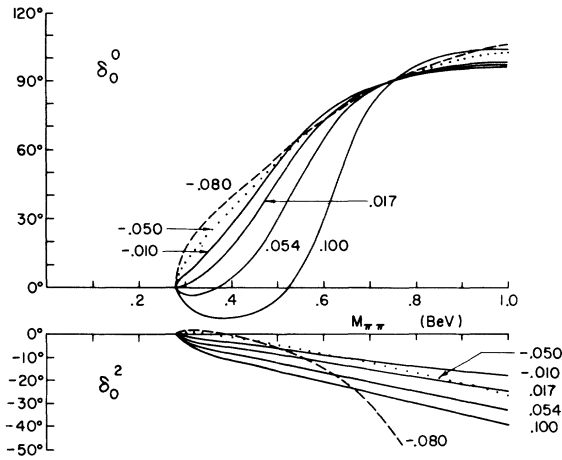


FIG. 1. s -wave phase shifts, labeled by λ , for typical solutions obtained when a σ of 745 MeV was required (method A).

choosing the set with $\alpha_0 < 0$, then minimizing the change in γ_0 resulted in solutions, while the opposite initial choice led to imaginary roots. However, for $\lambda < -0.008$ the initial roots were imaginary. This difficulty was overcome by assuming initial values for the $L_T(\nu)$ and their derivatives at the symmetry point taken from solutions obtained for the same λ values when the resonance was required. Even this technique failed for $\lambda < -0.033$, when after a few iterations the roots became imaginary.

III. RESULTS

Calculations were carried out for three cases. In the first, δ_0^0 was required to resonate at 745 MeV; in the second, δ_0^0 was fixed within its experimentally determined range near the ρ mass; in the third case, the third-derivative condition was imposed. In all cases λ was fixed *a priori* as a free parameter, and solutions were obtained over as wide a range of λ as possible. Crossing conditions through the second derivative were enforced in all cases.

A. Resonance Required

The s -wave phase shifts of typical solutions obtained when a σ of 745 MeV was required are shown in Fig. 1, and the related scattering lengths in Fig. 2. For $-0.05 < \lambda < 0.05$, the scattering lengths agree within 5% with the "universal curve" of Morgan and Shaw⁹ for a σ of 765 MeV. Thus, the general agreement found between their phase shifts and those of Fig. 1 is expected. Since the solutions presented here cover a wider range of λ , it is to be expected that as λ increases to 0.100 the sign change of δ_0^0 occurs at higher energy, and that

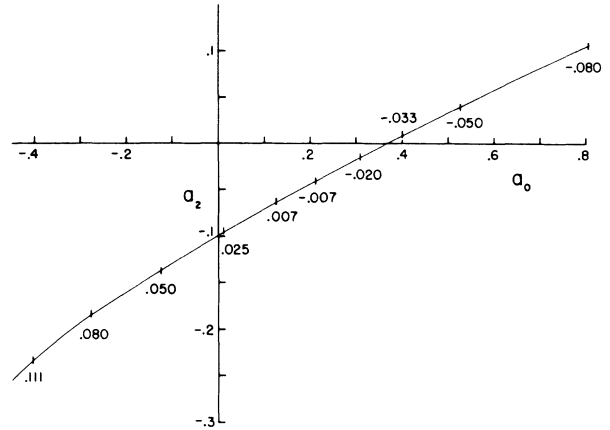


FIG. 2. s -wave scattering lengths, with λ values indicated, obtained when a σ of 745 MeV was required (method A).

as λ decreases to -0.080 , δ_0^0 increases more rapidly near threshold, than occurred in their limiting cases. Although they published no turnover δ_0^0 solutions, it may be assumed that they obtained them, since they obtained positive $I = 2$ scattering lengths for $\lambda < -0.03$. A notable difference, however, is seen when the δ_0^0 curves of Fig. 1 are compared with those of Morgan and Shaw near the σ resonance. Their solutions, obtained by treating the width of the σ as an input parameter, exhibit a wide range of widths, while the formalism used here predicts only very broad, asymmetric resonances. This result is in agreement with their conclusion that solutions with broad σ 's are preferable.

The third-derivative condition, Eq. (16), is plotted in Fig. 3. In order to display the results for a wide range of λ , the vertical scale has been com-

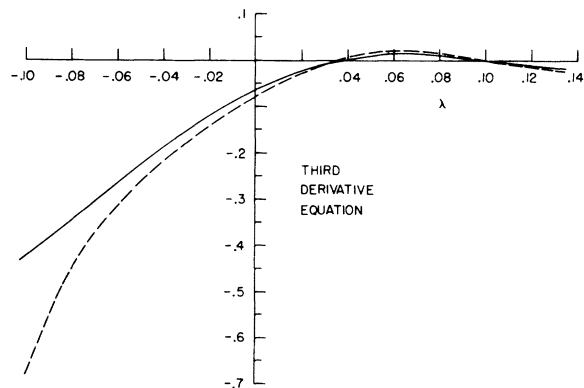


FIG. 3. Right- and left-hand sides of Eq. (16) as a function of λ for solutions obtained when a σ of 745 MeV was required (method A). The solid curve is the left-hand (s -wave) side and the dashed curve is the right-hand (p -wave) side.

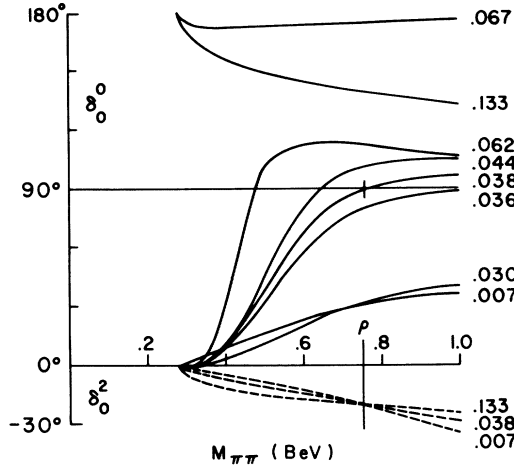


FIG. 4. Typical s -wave phase shifts for positive λ , obtained when $\delta_0^2 = -20^\circ$ at 745 MeV was required (method B). The solid curves show δ_0^0 and the dashed curves show δ_0^2 . Since the δ_0^2 curves interpolate smoothly between bounding solutions, some have been left out for clarity. All phase shifts are modulo π .

pressed, minimizing the visual impact of the intersection of these curves. Nevertheless, the curves clearly intersect, predicting "best" solutions with λ values of 0.03 and 0.10. In Fig. 1, for a solution with $\lambda = 0.03$, the value of δ_0^2 near the ρ mass would be about -19° , in acceptable agreement with recent estimates. (The other solution is discounted since its large negative α_0 and its δ_0^0 turnover above 500 MeV are contrary to experimental indications.)

Having demonstrated that the inverse amplitude formalism used here leads to sensible solutions when the σ is put in, it is hard to avoid asking whether or not other input can lead to solutions predicting a σ . A logical way to find out is to re-

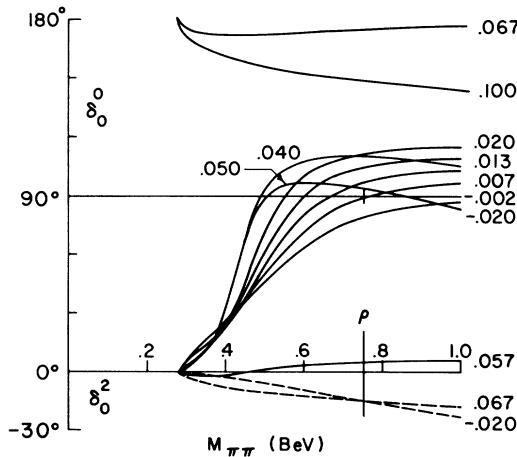


FIG. 5. Typical s -wave phase shifts, labeled by λ , obtained when $\delta_0^2 = -15^\circ$ at 745 MeV was required (method B). Solid and dashed curves are as in Fig. 4.

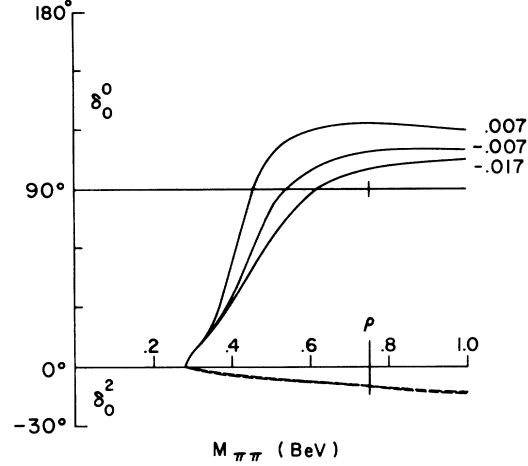


FIG. 6. Typical s -wave phase shifts, labeled by λ , obtained when $\delta_0^2 = -10^\circ$ at 745 MeV was required (method B). Solid and dashed curves are as in Fig. 4.

place the condition fixing δ_0^0 with one fixing δ_0^2 . The next section documents the results of such calculations.

B. δ_0^2 Fixed near the ρ

Figures 4–7 show the s -wave phase shifts of typical solutions obtained when⁸ the value of δ_0^2 at 745 MeV was fixed in its experimentally determined range. The reproducibility of results within this formalism may be seen as follows: From Fig. 1, a σ near the ρ mass is predicted for $\lambda \approx 0.04$ when $\delta_0^2 = -20^\circ$; it is seen in Fig. 4 for $\lambda = 0.038$. A similar σ may be expected for $\lambda \approx 0$ when $\delta_0^2 = -15^\circ$, and is seen in Fig. 5 for $\lambda = -0.002$. The incompat-

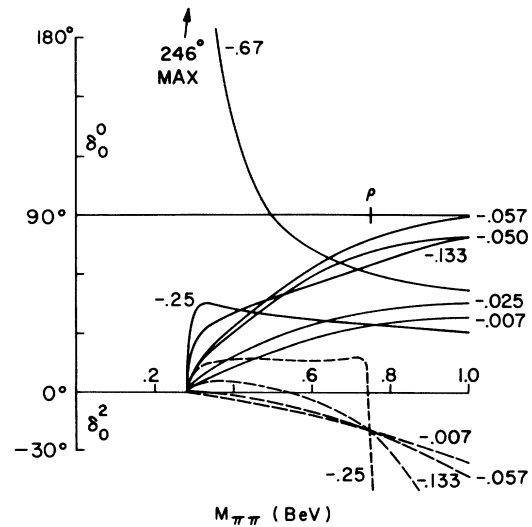


FIG. 7. Typical s -wave phase shifts for negative λ obtained when $\delta_0^2 = -20^\circ$ at 745 MeV was required (method B). Solid and dashed curves are as in Fig. 4.

ibility, seen in Fig. 1, of a σ near the ρ mass and $\delta_0^2 = -10^\circ$ is evident in the lack of such a solution in Fig. 6. Finally, for $\delta_0^2 = -20^\circ$ a σ near the ρ mass is predicted for $\lambda \approx -0.06$ from Fig. 1. Although such a result was not obtained, a solution for $\lambda = -0.057$, resonant at 1 BeV, is seen in Fig. 7. Thus the formalism is satisfactorily self-consistent.

The most obvious feature of Figs. 4–6, the decrease of the mass and width of the σ with increasing λ , turns out to be a misleading consequence of the constraint of δ_0^2 . The decrease would seem to imply an attractive interaction, increasing in strength with λ . However, the solution for $\lambda = 0.057$ of Fig. 5 shows that instead of a bound state being formed for large λ (i.e., the resonance approaching, then going below threshold with increasing λ) the interaction becomes repulsive. (Since intermediate solutions of this type most often failed to converge upon iteration, this conclusion was first reached by noting that the scattering lengths of Fig. 8 did not exhibit the discontinuity which would have corresponded to the establishment of a bound state.) The pertinent feature of these solutions is instead, the advance with increasing λ , of the pole of F_0^0 (zero of δ_0^0) toward $\nu = \infty$ and its reappearance at large negative values of ν .

The true increase of attraction occurs with negative λ , culminating in the formation of the bound state seen in Fig. 7 for $\lambda = -0.67$. However, only extremely heavy, broad σ 's are produced here, with the lightest occurring at 1 BeV for $\lambda = -0.057$. The close similarity of the solutions with $\lambda < -0.13$ to the negative λ solutions obtained in I is probably due to the constraint of the $I = 2$ s wave imposed in

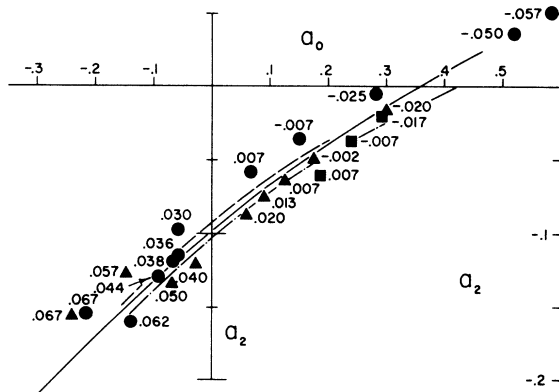


FIG. 8. s -wave scattering lengths of the solutions of Figs. 4–7 (method B). Values of δ_0^2 for solutions indicated by circles, triangles and squares are -20° , -15° , and -10° , respectively. The curves are from Ref. 2, a required σ of 900, 765, and 600 MeV yielding the upper, middle, and lower curves, respectively.

I by the insertion of a pole term into only the $I = 0$ s wave.

In Fig. 8 the s -wave scattering lengths are plotted one against the other. The curves are from Morgan and Shaw, with the upper, middle, and lower curves representing σ 's of 900, 765, and 600 MeV, respectively. The curve of Fig. 2, drawn for a σ of 745 MeV, would lie just slightly below the middle curve, as is expected. The progression of the points across the curves as the σ is established and moves toward threshold is in accordance with the ordering of the curves.

Order was introduced into this confusing welter of solutions by the third-derivative condition. Equation (16) applied to the various solutions, is shown in Fig. 9. It clearly selects a single solution from each set computed for a given δ_0^2 value. For δ_0^2 values of -10° , -15° , and -20° the preferred solutions have λ values of -0.017 , 0.007 , and 0.038 , and exhibit σ resonances with masses of 600, 660, and 750 MeV. Thus, with increasing λ the σ moves away from threshold, indicating a weakening attraction. The connection of these selected solutions with the repulsive solutions found in I for large positive λ is seen by the onset of repulsion indicated by the emergence of the pole of $F_0^0(\nu)$ (zero of

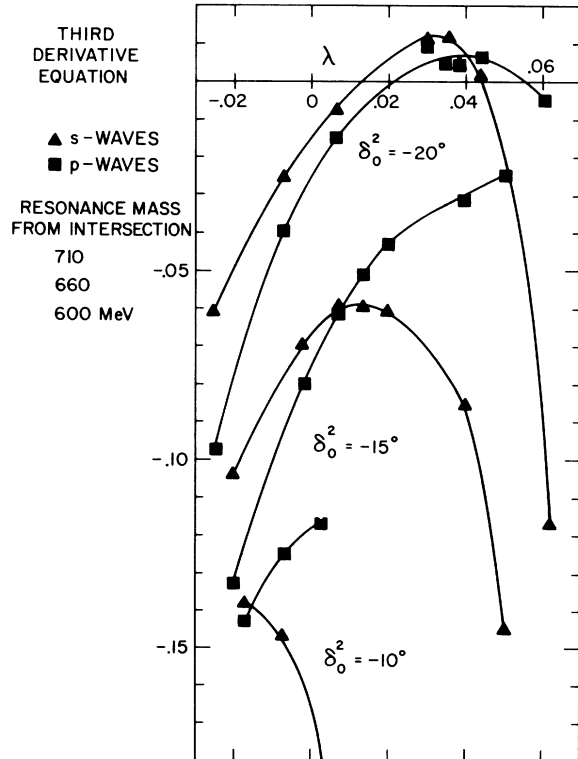


FIG. 9. Right- and left-hand sides of Eq. (16) as a function of λ for solutions obtained when δ_0^2 was fixed at 745 MeV (method B).

δ_0^0) above threshold in the solution for $\delta_0^2 = -20^\circ$ with $\lambda = 0.038$ (Fig. 4).

Thus, while restricting δ_0^2 allowed the prediction of σ resonances of various masses, a clear interpretation of the results required the additional imposition of the third-derivative condition from approximate crossing symmetry. With its usefulness thus proven, the next logical step was to see if it could be used in the determination of parameters during iteration. The results of such calculations are presented in the next section.

C. Third-Derivative Condition Imposed

The s -wave phase shifts for typical solutions obtained when all s -wave parameters were fixed by conditions from crossing symmetry are shown in Fig. 10. The attraction causing the resonant δ_0^0 's clearly weakens with increasing λ , and the solution with $\lambda = 0.10$ indicates the transition to the repulsive solutions previously obtained for $\lambda > 0.1$. The scattering lengths for these solutions agree closely with those computed when the resonance was required, and are plotted in Fig. 11. Imaginary roots obtained in solving for parameters prevented solutions with $\lambda < -0.033$ or $\lambda > 0.1$. Thus imposition of the third-derivative condition frees the formalism from the need of s -wave input from experiment, and leads to solutions having a sensible dependence on λ .

The locations of the zeros of the s -wave amplitudes are plotted one against the other in Fig. 12. For the resonant solutions, they lie on a straight line passing through the point predicted from PCAC considerations, which coincides with the solution with $\lambda = -0.008$. Since the resonant solu-

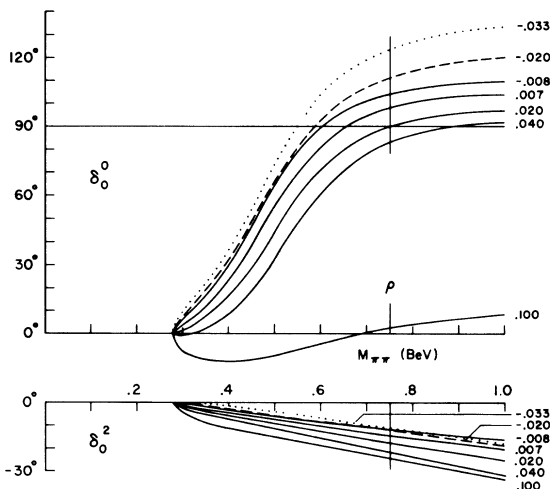


FIG. 10. Typical s -wave phase shifts, labeled by λ , obtained when Eq. (16) was imposed (method C).

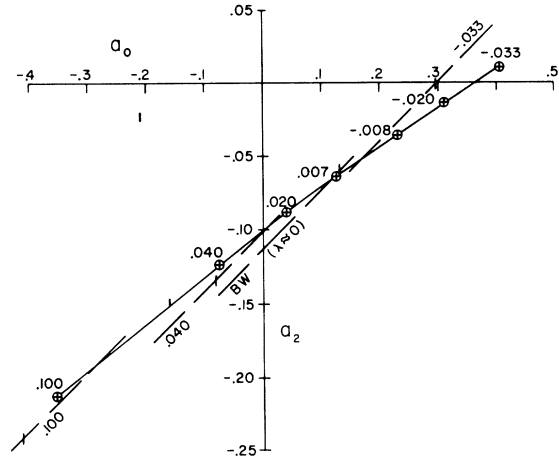


FIG. 11. The s -wave scattering lengths of the solutions of Fig. 10 (method C) are indicated by crosses, and labeled by λ values. Scattering lengths predicted by a linear extrapolation from the symmetry point of the s -wave amplitudes of these solutions are indicated by the vertical marks crossing the appropriately labeled dashed lines. These latter aspects of the figure are explained in the discussion after Eq. (30).

tions obtained for the other cases exhibited zeros lying on this same line, it was felt that this must be due to some invariant feature of the formulation. The most obvious possibility was a combination of the lowest-order crossing conditions. Parametrizing the s waves by

$$A_0^I(\nu) = a_I + b_I \nu, \quad (23)$$

and applying only Eqs. (12) to (14) yielded the prediction

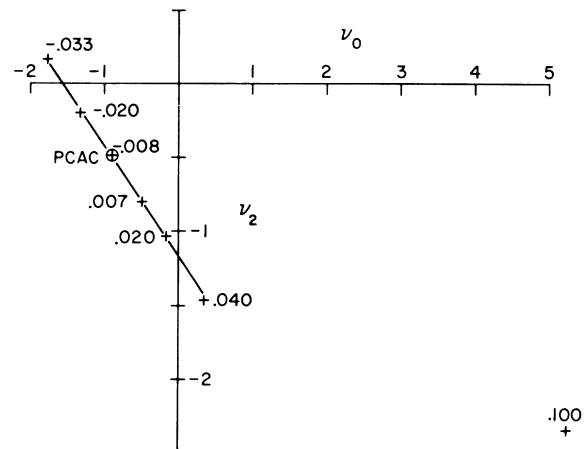


FIG. 12. Zeros of the s -wave amplitudes of the solutions of Fig. 10 (method C) labeled by λ values. Weinberg's prediction is labeled PCAC and coincides with the solution for $\lambda = -0.008$. The straight line is seen to pass through the points.

$$\nu_2 = -0.8\nu_0 - 1.2 \quad (24)$$

for comparison with the line of Fig. 12,

$$\nu_2 = 0.740\nu_0 - 1.17. \quad (25)$$

Since the calculated amplitudes are not linear, this is quite satisfactory agreement. The difference in slopes is mainly due to a systematic decrease, with increasing λ , of the second derivative of A_0^0 at the symmetry point.

In achieving the above prediction, it was seen that, in addition, the scattering lengths would be related by

$$2a_0 - 5a_2 = 18/F_1^1(sp) \quad (26)$$

(still assuming linear s waves). The Breit-Wigner (B-W) ρ used to fix the p wave in Eqs. (9) and (10) corresponds to $F_1^1(sp) = 31.9$, so the scattering lengths would lie on the line

$$a_2 = 0.4a_0 - 0.113. \quad (27)$$

Now in the actual calculations, the p wave differs from a B-W resonance due to the cut integrals. Examination of the solutions shows that $F_1^1(sp)$ increases with λ , and agrees with the B-W value for $\lambda \approx 0$. For each solution it is straightforward to predict a line similar to Eq. (27) and (using the value of λ also) the point on the line expected if the s -wave amplitudes were linear. These predictions are shown in Fig. 11. From the surprising accuracy of these crude predictions it is clear that the scattering length curve is determined primarily by the lowest-order crossing conditions and the p wave at the symmetry point.

The asymmetry of the δ_0^0 curves makes it difficult to assign widths to the σ 's indicated by the various curves. A common approximation is to quote the width of a Breit-Wigner resonance, the real part of whose inverse amplitude at the resonance position has the same slope. For the solutions with $\lambda = -0.033$, 0.007 , and 0.040 , above the resonance the square of such an amplitude falls to half of its maximum value at 710, 1050, and 2350 MeV. However, the corresponding point below the resonance lies below threshold for all solutions except that for $\lambda = -0.033$, for which it lies at 310 MeV.

Resonance width is also often related to the position of an unphysical-sheet pole of the scattering amplitude. When the variable ν of Eq. (2) is allowed to become complex, a zero of $F_I(\nu)$ indicates a pole of A_0^I . The sheet structure of A_0^I is such that continuation above the real axis is onto the nearby physical sheet, while continuation below the real axis is onto the unphysical sheet. In searching for complex zeros of $F_I(\nu)$, various fits to the functions were made on the real axis to facilitate

continuation. For $\lambda = 0.007$ a zero corresponding to a pole of A_0^0 was found variously from $\nu = 1.6 - 1.6i$ to $\nu = 2.4 - 3.5i$. No attempt was made to iterate or refine the pole position because it is clearly far from the physical sheet and narrow-resonance formulas are no longer applicable. It is worth noting, however, that neither A_0^0 nor A_0^2 were found to have poles on the nearby physical sheet by this procedure.

An indication of self-consistency is provided by comparing A_0^I for $\nu < 0$ as calculated from the crossing integral of Eq. (7) and from $\text{Im}F_I$. These quantities are plotted in Fig. 13 for the solution with $\lambda = -0.008$ which is typical of solutions in the range $-0.01 < \lambda < 0.025$. The agreement is seen to be excellent out to $\nu = -6.5$; beyond this point the curves diverge toward the different asymptotic behaviors discussed in Ref. 3. Consequently, for these solutions an upper limit of validity in the physical region may be inferred at roughly the energy of the ρ resonance. Examination of Fig. 12 shows that for $\lambda < -0.01$ the pole of F_0 has moved onto the left cut and for $\lambda > 0.025$ the pole of F_2 has done likewise. In the vicinity of such poles, values of $\text{Im}A_0^I$ calculated from $\text{Im}F_I$ become very small in contrast to values calculated from the crossing integral which remain similar to the solid curve of Fig. 13. Although the discrepancy is found only in the immediate vicinity of the poles, the lack of self-consistency on the nearby left cut makes the validity of these solutions questionable. Further

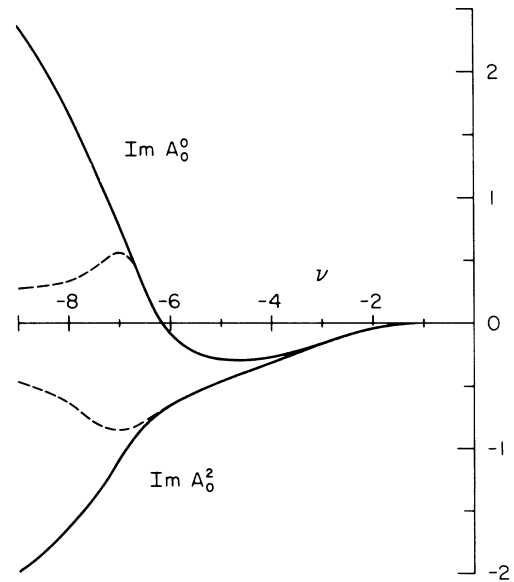


FIG. 13. Imaginary part of the s -wave amplitudes for $\nu < 0$ for the solution with $\lambda = -0.008$. The solid curves are from crossing and the dashed curves are from the inverse amplitudes.

discussion will therefore be limited to solutions not affected by this problem.

IV. DISCUSSION

It is seen that all solutions having zeros of both s -wave amplitudes between the cuts ($-0.01 < \lambda < 0.025$) exhibit broadly resonant $I=0$ s waves. Since $\text{Re}F_0$ falls from $+\infty$ between the cuts through zero at the resonance position, a more rapid increase of δ_0^0 above the resonance mass is clearly possible within the present formalism. However, a further rise through 180° as used by Bizzari¹⁰ in fitting experimental data is precluded by the present formalism (an additional pole term would be required in F_0 to allow δ_0^0 to reach 180° for finite ν). While the present calculations therefore yield no information on the existence of such structure in F_0 above the ρ mass, it is noted that the inclusion of such effects would have little effect on results at lower energies.¹¹

Tryon¹² has raised the possibility that the $A_0^I(\nu)$ contain infinitely many complex zeros on the physical sheet, with an accumulation point at infinity, which would cause poles of the F_I in addition to those below threshold. While the constant contributions of such poles are automatically absorbed into subtraction constants, higher-order terms are not. From the nearest poles, Tryon has estimated a linear contribution to $F_0(\nu)$ which increases to 0.22μ at 750 MeV. Since the formalism used here is based upon the assumption that such poles either do not exist or can be neglected, it provides no information regarding this possibility. The reader is cautioned, however, against using this estimate to infer changes in the δ_0^0 values here presented. The contribution of the subthreshold pole term to $F_0(\nu)$ at 750 MeV ranges from three to six times Tryon's estimate for solutions with $-0.01 < \lambda < 0.025$. Since the evaluation of the pole-term parameters would clearly be affected by any attempt to incorporate a linear term into $F_0(\nu)$, there is no straightforward way to predict the effect of such an attempt on δ_0^0 . No further discussion of this

point will be attempted here.

Our solutions for $A_0^I(\nu)$ contain no ghost poles on the nearby physical sheet, since our $F_I(\nu)$ contain no complex zeros in this region, as has already been noted.

The determination of parameters through derivative conditions from approximate crossing symmetry introduces errors caused by the truncation of partial-wave series in the derivation of Eqs. (12)–(16). While waves higher than p were neglected in writing Eqs. (12)–(14), the effects of higher waves upon the second- and third-derivative conditions were minimized by including parametrized threshold fits which were then removed by combining equations. It is possible to show *a posteriori* that the d and f waves are small, even with respect to the small s waves associated with small values of $|\lambda|$ [recall $A_0^0(sp) = -5\lambda$]. The equations which were combined to remove the effects of those waves in deriving Eqs. (15) and (16) have been used to calculate their values at the symmetry point from the s - and p -wave solutions presented in Sec. III C.¹³ Even though the s -wave amplitudes vanish with λ , for each isospin state the magnitude of the d -wave amplitude is less than 4% of the magnitude of the s -wave amplitude for all of the solutions of Fig. 10, and this decreases to 1% for solutions with larger values of $|\lambda|$. More important, however, is how this affects the value of A_0^2 as calculated from $\lambda = -\frac{1}{5}A_0^0$ (evaluation at the symmetry point is implied throughout this discussion). When d and f waves are included in Eq. (12) the value of A_0^2 is changed by

$$\Delta(A_0^2) = -(A_2^0 - \frac{5}{2}A_2^2). \quad (28)$$

The change for each of the solutions of Fig. 10 is listed in Table I, and in no case exceeds 2%.

For each of the solutions of Fig. 10 the f -wave amplitude is less than $\frac{1}{2}\%$ of the p -wave amplitude (at the symmetry point). Although it does not affect Eq. (28), it does affect the derivative conditions for the s waves, which also involve the slopes of the d waves. For each isospin state, the slope of the d -wave amplitude ranges from $2\frac{1}{2}\%$ to 1% of

TABLE I. Symmetry-point values of s -wave amplitudes and their derivatives for the solutions of Fig. 10 (method C). Also, the changes in these quantities computed *a posteriori* due to inclusion of d - and f -wave contributions (A_0^0 is related to λ , and hence does not change).

λ	A_0^0	A_0^2	$\Delta(A_0^2)$	$\frac{dA_0^0}{d\nu}$	$\Delta\left(\frac{dA_0^0}{d\nu}\right)$	$\frac{dA_0^2}{d\nu}$	$\Delta\left(\frac{dA_0^2}{d\nu}\right)$
-0.033	0.167	0.0667	0.0003	0.200	-0.015	-0.1000	-0.0036
-0.020	0.100	0.0400	0.0001	0.196	-0.013	-0.0978	-0.0036
-0.008	0.040	0.0160	0.0001	0.191	-0.011	-0.0956	-0.0036
0.007	-0.033	-0.0133	-0.0002	0.184	-0.010	-0.0922	-0.0023
0.020	-0.100	-0.0400	-0.0008	0.177	-0.008	-0.0887	-0.0003
0.040	-0.200	-0.0800	-0.0006	0.169	-0.006	-0.0843	-0.0025

the slope of the s -wave amplitude (at the symmetry point) for the solutions of Fig. 10. When d and f waves are included in Eqs. (13) and (14) the symmetry-point slopes of the s waves are changed by

$$\Delta\left(\frac{dA_0^0}{d\nu}\right) = \frac{63}{2}A_3^1 + \frac{5}{2}\frac{dA_2^0}{d\nu} \quad (29)$$

and

$$\Delta\left(\frac{dA_0^2}{d\nu}\right) = -\frac{63}{4}A_3^1 + \frac{5}{2}\frac{dA_2^2}{d\nu}. \quad (30)$$

[The large factor multiplying the f -wave contributions in these equations is misleading – note the p -wave multiplier in Eqs. (13) and (14).] These changes are also listed in Table I for the solutions of Fig. 10. The contributions to Eq. (30) tend to cancel, yielding a maximum change of 2% for the $I=2$ s -wave slope, while the contributions to Eq. (29) tend to add. The percent change of the $I=0$ s -wave slope decreases from $7\frac{1}{2}\%$ for the solutions with $\lambda = -0.033$ to $3\frac{1}{2}\%$ for the solution with $\lambda = 0.040$.

Although higher partial waves have been removed in the derivations of Eqs. (15) and (16) the restricted nature of the parametrization may also introduce errors. For instance, while in deriving Eq. (16) the f wave is written as

$$A_3^1(\nu) = c\nu^3, \quad (31)$$

one may ask how the satisfaction of Eq. (16) would be affected if the f wave were given by

$$A_3^1(\nu)' = a\nu^3 + b\nu^4 \quad (32)$$

with the same magnitude at the symmetry point and $a/b=3$. When Eq. (16) is rederived keeping f waves in general, and then the form of Eq. (32) is substituted in with parameters evaluated in terms of the calculated value of A_3^1 at the symmetry point, the result is [we denote the left-hand and right-hand sides of Eq. (16) by L and R , respectively]

$$L = R + \delta, \quad (33)$$

where

$$\delta = \frac{675}{4}A_3^1. \quad (34)$$

The results calculated from the solutions of Fig. 10 are presented in Table II where the p -wave side of Eq. (16) is seen to be shifted by about 10%. If $a/b = -3$ the δ has the opposite sign and is about half as large.

While it should be possible to remove the errors in the magnitudes and slopes of the s waves by incorporating d -wave effects into Eqs. (12)–(14) in an iterative manner, refinement of the second- and third-derivative conditions will require better

knowledge of the d and f waves, perhaps through iterated dispersion relations utilizing present s - and p -wave solutions in the calculation of left-cut integrals. The success of the present formalism in achieving sensible solutions makes it desirable to pursue such calculations. Consequently the possible effects of f -wave behavior on solutions selected by the third-derivative condition are now discussed. As seen in Eqs. (33) and (34) the effect of unanticipated structure in the f wave is to introduce a correction to the right-hand (p -wave) side of Eq. (16) which is proportional to the symmetry-point value of the f -wave amplitude. Inspection of Table II yields the fact that the correction is essentially a constant percentage of the p -wave side of Eq. (16). The effect of including such a correction in the formalism may be seen by shifting the p -wave curves of Fig. 9 appropriately, then identifying the solutions of Figs. 4, 5, and 6 which correspond to the λ values for which the curves of Fig. 9 intersect. Roughly, a 10% lowering of the p -wave curves of Fig. 9 (corresponding to the ratio $a/b=3$) results in a 10% decrease in the mass of the predicted σ resonance for $|\lambda| < 0.02$. A 30% lowering ($a/b=1.4$) causes 20% decrease in σ masses. A 10% raising of the p -wave curves ($a/b=-1.7$) results in a 10% increase in the σ masses for $|\lambda| < 0.02$.

From the uncertainties documented above it is clear that an accurate application of derivative crossing conditions requires considerable care. This, of course, accounts for the popularity of the inequalities of Martin¹⁴ which are less sensitive to truncation of the partial-wave series. It is therefore of some interest to compare the solutions presented here with the results of independent calculations, also based on inverse amplitude dispersion relations, which use Martin's inequalities to evaluate parameters.¹⁵ In those calculations the s waves were represented by functions similar to the $F_I(\nu)$ of this paper. The six s -wave parameters were fixed by matching the $F_I(\nu)^{-1}$ below threshold to solutions for $A_0^I(\nu)$ obtained from quadratic polynomial approximations to the amplitudes. The

TABLE II. Changes of the right-hand (p -wave) side of Eq. (16) when the f -wave parametrization is changed; ($a/b=3$) as discussed in the text.

λ	Eq. (16)	$10^4 A_3^1$	δ	%
0.040	0.008	0.05	0.0008	10
0.020	-0.025	-0.11	-0.0019	8
0.007	-0.061	-0.34	-0.0057	9
-0.008	-0.110	-0.59	-0.0100	9
-0.020	-0.147	-0.86	-0.0145	10
-0.033	-0.193	-1.1	-0.0186	10

assumption that the Adler condition holds on the mass shell caused zeros of the s -wave amplitudes to coincide in all cases with those of the solution for $\lambda = -0.008$ presented here. The solutions of Ref. 15 are ordered by a free parameter X ; constraining X to positive values caused the polynomial amplitudes to satisfy eight conditions placed on the $\pi^0\pi^0$ scattering amplitudes. Solutions with $0.7 \leq X \leq 0.5$ were preferred on the basis of agreement with experiment; the solution with $X = 0.7$ is in good agreement with the solution here presented for $\lambda = -0.008$. Since the s waves of both solutions are similarly parametrized and have subthreshold zeros at coincident points one might expect that the crossing conditions used in Ref. 15 were satisfied by the $\lambda = -0.008$ solution. Of the eight conditions,¹⁶ only the sixth and seventh were unsatisfied, by 20% and 10%, respectively. All conditions were satisfied by the solution with $\lambda = -0.020$, while the solution with $\lambda = 0.007$ was less satisfactory. One may speculate that a more careful treatment of higher waves might induce changes in the solutions presented here which were somehow related to the lack of satisfaction of these conditions. If so, the greatest changes would be expected in solutions with $\lambda > 0$, perhaps even yielding nonresonant solutions for realistically small values of λ . The significance of this possibility lies in the existence of such solutions in the literature.⁷ It is possible that differences in the behavior of various solutions near the ρ mass may be mainly due to differences in the details of application of approximate conditions near and below threshold.

In summary, the solutions presented in Fig. 10 are known to contain errors due to approximations made in the derivation of derivative conditions from crossing symmetry which are used in the evaluation of s -wave parameters. However, solutions with $\lambda \leq -0.01$ satisfy a set of crossing conditions derived so as to be insensitive to higher partial waves, and the solutions with $\lambda = -0.008$ are in good agreement with independent results obtained without using derivative conditions. Thus the solutions with lower mass σ resonances may

change little under improvement of the formalism. The imposition of derivative conditions to third degree from crossing symmetry is seen to provide a formalism which produces s -wave solutions above threshold with a sensible behavior as a function of λ , which also indicates a connection to earlier nonresonant solutions. In addition zeros of both s -wave amplitudes are found. The positions of the zeros are linearly related, and one solution has zeros which coincide with those obtained when the (off-mass-shell) Adler condition for PCAC is assumed to hold on the mass shell. The zeros appear naturally from the imposition of the crossing conditions, in the absence of any input from PCAC—in fact the only input to the calculation is the requirement that the p wave exhibit a resonance of mass 755 MeV and width 120 MeV, which is used to fix the p -wave subtraction constants.

In order to improve the accuracy of the predictions of this model the following future modifications are proposed. First, the d - and f -wave modifications to the zeroth- and first-derivative equations indicated in Eqs. (29)–(31) should be incorporated in the determination of parameters in an iterative way. Second, more accurate estimates of the d and f waves at the symmetry point should be obtained using dispersion relations incorporating the s - and p -wave results. These results should then be incorporated into the application of all derivative conditions used in the determination of s -wave parameters in an iterative way. Efforts are being initiated toward the accomplishment of these objectives.

ACKNOWLEDGMENTS

It is a pleasure to acknowledge many discussions with Claude Kacser. The author is grateful to the National Science Foundation's Research Participation Program for College Teachers for the opportunity to carry out this investigation. The hospitality of the faculty and staff of the Center for Theoretical Physics, and of the Computer Science Center of the University of Maryland is also greatly appreciated.

*Supported in part by the National Science Foundation under Grants No. NSF GY-5461 and NSF GY-8541. Computer time was furnished by the University of Maryland Computer Science Center under NASA Grant No. NSG-398. The author was a visitor at Stanford Linear Accelerator Center during revision of the manuscript.

¹S. Weinberg, Phys. Rev. Letters **17**, 616 (1966).

²G. F. Chew, S. Mandelstam, and H. P. Noyes, Phys. Rev. **119**, 478 (1960).

³B. H. Bransden and J. W. Moffat, Nuovo Cimento **21**,

505 (1961); Phys. Rev. Letters **8**, 145 (1962); Nuovo Cimento **32**, 159 (1964).

⁴K. Kang, Phys. Rev. **134**, B1324 (1964).

⁵B. F. Gore, Phys. Rev. **183**, 1431 (1969).

⁶G. F. Chew and S. Mandelstam, LRL Report No. UCRL 9126, 1960 (unpublished).

⁷E. P. Tryon, in *Proceedings of a Conference on $\pi\pi$ and $K\pi$ Interactions at Argonne National Laboratory*, edited by F. Loeffler and E. D. Malamud (ANL, Argonne, Ill., 1969); Phys. Rev. Letters **20**, 769 (1968).

⁸In evaluating the numerical integrals the integration variable was changed to $(\nu+1)^{-1/2}$ for $\nu > 0$ and $(-\nu)^{-1/2}$ for $\nu < -1$, and the unit interval of integration was divided into forty equal subintervals for evaluation by Simpson's rule. This grid, extremely fine near threshold and growing coarser with increasing $|\nu|$, allows a more accurate evaluation of the better-known contributions near threshold. It was convenient to impose conditions at grid points, and the grid point closest to the ρ mass was at 745 MeV.

⁹D. Morgan and G. Shaw, Nucl. Phys. **B10**, 261 (1969); Phys. Rev. D **2**, 520 (1970).

¹⁰R. Bizzari *et al.*, Nucl. Phys. **B14**, 169 (1969).

¹¹Right-cut effects occurring for $\nu > \nu_1$ only affect the left-cut integrand through Eq. (7) for $\nu < -(\nu_1 + 1)$. Since the left-cut integral is subtracted, the effects of distant variations in its integrand are minimized. This argu-

ment, plus the fact that by all estimates d waves are thought to be small below (at least) the ρ mass, justifies the truncation of the integrand of Eq. (7) after p waves.

¹²E. P. Tryon, Phys. Rev. D **4**, 1216 (1971).

¹³ d waves were calculated using both the one-parameter and two-parameter d -wave threshold fits used to derive Eqs. (15) and (16). Results agreed within 10–20% for both magnitudes and slopes. Central values are used in the following discussion.

¹⁴A. Martin, Nuovo Cimento **47**, 265 (1967); A. K. Compton, *ibid.* **53A**, 946 (1968).

¹⁵J. B. Carrotte and R. C. Johnson, Phys. Rev. D **2**, 1945 (1970).

¹⁶Equations (20) to (27) of R. H. Graham and R. C. Johnson, Phys. Rev. **188**, 2362 (1969), applied to quadratic fits to the s waves.

PHYSICAL REVIEW D

VOLUME 6, NUMBER 2

15 JULY 1972

Magnetic Dipole Moment of the Electron in the Ladder Approximation*†

John M. Zavada, Jr.

Department of Physics, New York University, New York, New York 10003

(Received 7 December 1971)

In order to calculate the magnetic dipole moment of the electron in a nonperturbative manner, the vertex function of quantum electrodynamics is studied in the ladder approximation. The vertex function is written as the sum of form factors and coupled, linear integral equations are derived for these form factors. After converting the system of integral equations into differential equations, the form factors are expressed by means of an infinite series. By using the leading term in the series solution, an approximation for the magnetic dipole moment of the electron is obtained. This nonperturbative approximation is considered in the limit of a large coupling constant, g , and the electric dipole moment, μ_E , of a magnetic monopole with mass M is found to be $\mu_E \sim [\sqrt{2}(4\pi)^2 g^{-5/2}] g/2M$. Assuming the neutron to be a bound state of magnetic monopoles, the electric dipole moment of the neutron is estimated as being $10^{-18} e$ cm.

I. INTRODUCTION

From its inception, quantum electrodynamics has been closely associated with a perturbation expansion in terms of the fine-structure constant α . The first calculations in quantum electrodynamics were of the leading term in this expansion and, surprisingly, gave results which were in good agreement with experiments. Later, when the divergences in the higher-order terms were explained and removed by the Dyson-Salam technique¹ of renormalization, it was possible to calculate processes to an even greater degree of accuracy. The accuracy to which theoretical predictions for processes such as the Lamb shift and the magnetic dipole moment of the electron agree with experiments is quite remarkable.² However, these calculations are valid only in a perturbation theory and no one has been able to show that such an expansion does converge or that the remaining high-

er-order terms are, in fact, negligible.

When the magnitude of the coupling constant is small, as it is in quantum electrodynamics, one may be somewhat content in being able to calculate only the leading terms in a given process. However, a perturbation treatment makes no sense when the coupling constant is large as it is in the strong interactions and in the interactions of magnetic monopoles.

Dirac postulated the existence of magnetic monopoles, particles with magnetic charge, in order to explain the appearance of only integral electric charges in nature.³ With the inclusion of magnetic charge, Maxwell's equations become completely symmetric with respect to electric and magnetic quantities. Furthermore, the properties of the monopoles will be symmetric with the properties of the electrons under the interchange of electric and magnetic terms. For example, in an external electromagnetic field, the electron will possess a